Removal of humic acid by coagulation with nano-Al_{13}

W. Dongsheng*, L. Hong*,, L. Chunhua* and T. Hongxiao***

*SKLEAC, Research Center for Eco-Environmental Science, Chinese Academy of Sciences, Beijing, 100085, China (E-mail: *wgds@mail.rcees.ac.cn*)

**Department of Chemistry, Beijing University of Science and Technology, Beijing 100083, China

Abstract Pure Al_{13} solutions at various concentrations were prepared by using the SO_4/Ba separation method and characterized by using ^{27}Al-NMR, IR, PCS, AFM and Ferron assay. The mechanism of humic acid removal by coagulation with Al_{13}, lab-made PACl and industry PACl was compared. Special attention has been paid to the aspects of different coagulation species. The influence of pH and dose was discussed respectively from the change of zeta potential, residue turbidity, and UV_{254}. The results show that the Al_{13} is the dominant and important species in the coagulation process deciding the charge-neutralization ability.

Keywords Al_{13}; coagulation mechanism; humic acid; polyaluminium chloride

Introduction

In aqueous solution, Al(III) exhibits strong trend of hydrolysis. After dosing into water solution, it will undergo serial hydrolysis, polymerization, aggregation and precipitation process. As results, various possible species existing in a metastable or transient state could be formed in the bulk solution. Among them, the Al_{13} species has received more and more attention. The application of Al_{13} has been engaged in many fields such as water and wastewater treatment, manufacture of pharmaceuticals, main components in certain catalysts, and modification reagents for soil (Parthasarathy and Buffle, 1985; Parker and Bertsch, 1992; Furrer, 1993; Gray *et al.*, 1995; Bertsch, 1996; Matsui *et al.*, 1996). It has also been considered to play a significant role in the case of acid precipitation and global chemical recycling. Especially in water treatment, the polyaluminium chloride (PACl) has been rapidly developed based on the traditional metal salts, the Al_{13} or Al_b as shown in the ferron assay were considered to be the most important species.

PACl as one of the main kinds of inorganic polymer flocculants (IPFs) exhibits high coagulation efficiency and has been widely applied both in water and wastewater treatment. During the last decades, the mechanism of coagulation with PACl has been extensively investigated and gradually recognized (Teagarden *et al.*, 1981; Pinnavia, 1983; Furrer, 1993; Gray *et al.*, 1995; Tang and Luan, 1996; Tang, 1998; Wang *et al.*, 2002; Wang *et al.*, 2004). However, some argument and uncertainty remain unsolved. It is because of the nature of the PACl solution containing various species. The speciation component and particle size distribution in the PACl solution depend largely on the basicity (B, OH/Al ratio), total aluminium concentration, pH value, and the preparation technology as well. The various species play significantly different roles during the coagulation process.

The research above mentioned is mostly based on the partially alkalinized Al(III) solutions. The results obtained are unavoidably the co-effect of all the various species, and Al_{13} is only one of the main species. The knowledge towards better understanding of the formation mechanism, structure morphology, physicochemical property and coagulation mechanism of the various hydrolysed polymer species remains to be exploited. Meanwhile, the quality of industrial PACl products varied significantly. The content of Al_{13}

Water Science and Technology: Water Supply **Vol 6 No 1 pp 59–67** © IWA Publishing 2006

doi: 10.2166/ws.2006.007

remained very low and the process for PACl products still lacked a reliable quality index (Pinnavia, 1983; Van Benschoten and Edzwald, 1990; Furrer, 1993; Tang, 1998; Wang *et al.*, 2002). Therefore, purified Al_{13} species are greatly needed to examine experimentally the mechanism of coagulation with IPFs. Methods to separate the various species in the hydrolysed solutions are needed. And it becomes one of the hot topics in this area. The objective of this paper is to investigate the possibility of preparation of Al_{13} nano-flocculant and characterize pure Al_{13} solutions at various concentrations by using the ^{27}Al-NMR, IR, AFM and Ferron assay in combination. The optimum process for the separation and purification of Al_{13} has been established (Van Benschoten and Edzwald, 1990). In this paper, the mechanism of coagulation with Al_{13} in presence of humic acid (HA) is further investigated. A comparison of coagulation among Al_{13}, lab-PACls and industrial PACl products was studied. Special attention has been paid to the aspects of different coagulation species. The influence of pH and coagulant dose was discussed respectively from the change of zeta potential, residual turbidity (RT), and UV_{254}.

Materials and methods

Preparation of lab-PACl and Al_{13} nano-flocculant

The preparation of lab-PACl and Al_{13} solution was adopted as in the literature (Pinnavia, 1983; Van Benschoten and Edzwald, 1990). The various PACl samples were prepared by using a slow base titration method at room temperature. A solution of $AlCl_3{\cdot}6H_2O$ was titrated slowly with NaOH at the target OH/Al ratio (B values). The chosen B values were 0, 2.0 and 2.5, and the resulting samples were denoted respectively as $PACl_0$, $PACl_{20}$ and $PACl_{25}$. The final concentration of Al was 0.1 mol/L. The samples after aging for one week were analyzed by an assay procedure using ferron reagent.

The purification of Al_{13} has been shown in the literature (Van Benschoten and Edzwald, 1990). Batches of purified Al_{13} samples were mixed together and freeze-dried to white solid powder. Different purified Al_{13} solutions were then prepared by diluting a certain amount of the powder into distilled water to the desired concentrations, i.e., 0.01, 0.05, 0.1, 0.5, 1.0, and 2.0 mol/L respectively. The total aluminium concentration and speciation distribution were further characterized by using ferron assay, ^{27}Al-NMR, IR, PCS, and AFM.

The industrial PACl (denoted as $PACl_{ind}$) products were provided by the local plants, Wanshui Water Treatment Reagent Company, Beijing. Certain amount of the PACl solution was diluted using de-ionized water to 0.1 mol/L before experiments. The results for ferron assay are shown in Table 1.

Speciation methods

Al-Ferron assay. The basic procedure of ferron assay has been addressed elsewhere in the literature (Pinnavia, 1983; Xu *et al.*, 2003). 5.5 ml of the pre-mixed ferron solution was pipetted into 25 ml graduated glass tube and then diluted into the marked line with distilled water. The samples were added by using a micropipette and mixed rapidly. After homogeneous mixing, the reacting sample was quickly added to a 1 cm glass cuvette.

Table 1 Characterization of speciation distribution of various coagulants

B	PACl	Al_a%	Al_b%	Al_c%
0	$PACl_0$	91.30	9.70	0
2.5	$PACl_{25}$	8.73	74.87	16.4
2.46	Al_{13}	2.72	97.02	0.26
1.62	$PACl_{ind}$	38.50	34.44	27.06

The timed absorbance measurements (at 366 nm), using a DU650 Beckman UV-Visible spectrophotometer, were carried out after 1 min and recorded for further 2 h. It was operationally divided that the 1 min absorbance as Al_a, and 1 min to 2 h as Al_b, then Al_c was obtained by Al_t minus Al_a and Al_b.

^{27}Al-NMR analysis. The solution was examined by using 500 MHz ^{27}Al NMR spectroscopy (Advance drx500 Bruker, Germany). The experimental conditions are: NS = 128, P1 = 14.00 μs, $PL_1 = -3.00$ dB, O_1P:47.38; DW:19.20, Solvent: D_2O, and T = 298 K. The standard used is 0.05 mol/l $NaAlO_2$ (with 75% D_2O).

AFM characterization. The AFM used was a NanoScope IIIa Multimode Scanning Probe Microscopy Instrument (Digital Instruments, Santa Barbara, CA) equipped with an E-scanner operating in air at room temperature with 50–60% humidity. The images presented in this paper contain 256 × 256 data points (pixel resolution), acquired by using the retrace signal either in the contact mode or in the tapping mode AFM. For the contact mode, the standard V-shaped silicon nitride (Si_3N_4) cantilevers (with integral tips, Model OTR8-35) of different stiffness and tip sharpness were used for imaging. Their nominal dimensions were 100 and 200 μm in length and 0.8 μm in thickness and possessed a spring constant ranging from 0.06 to 0.58 Nm^{-1}. For the tapping mode, the silicon cantilevers with 125 μm in length and 300 kHz in frequency (Nanoprobe, Model:RTESP14) were employed. The scanning speed and the loop gain factors were varied during the imaging process. Line scan rates were typically set at about 2.5 Hz for contact mode and 1.0 Hz for tapping mode with other scan parameters such as scan size, set point, integral gain, proportional gain etc. varied and optimized. In order to avoid tip-related artifacts, imaging was performed with a minimal force and image features were reproduced before being accepted as representative. For each experimental condition, two mica sheets were prepared and at least three images were obtained for each mica sheet sample. The prepared samples were investigated within a few hours of preparation by contact or tapping mode AFM observation. Images were taken with online filtering and subsequently by flattening to remove the background slope. Using NanoScope image analysis software, section analysis of images was conducted to measure the size of particles and their aggregates.

During the AFM imaging, a modified approach of drop deposition method, i.e. electrostatic deposition, was used. Aliquots of Al_{13} solutions (20 μl) were pipetted onto the fresh basal-plane surfaces of mica and left undisturbed for 5 min followed by a gentle rinse with ultra-pure water to remove any non-adsorbed and loosely attached substances. After the washing procedure excess water droplets adhering to the mica surface were carefully blown away using a stream of compressed air, and the mica was then allowed to dry in an enclosed Petri dish under ambient conditions before being placed onto the AFM stage.

IR characterization. The IR characterization was carried out by using NEXUS 670X. 1–2 mg of the samples were mixed with 100 mg KBr as carrier. Under a pressure of 10 atm, the samples were made into transparent slice. It should be noted that the samples and KBr must be dried before preparation.

Coagulation experiments

A stock suspension of purified kaolin (Imerys, UK) was prepared in deionized water (Elgastat Option 3 system) to a concentration of 100 g/L. It is known that kaolin particles undergo self-aggregation when the solution pH is decreased below about 4. Working

suspensions were prepared by diluting the above stock suspension in a test solution containing 5×10^{-4} mol/L $NaNO_3$ and $NaHCO_3$, respectively, to provide fixed concentrations of electrolyte and alkalinity.

For the coagulation tests, a modified jar test procedure was applied allowing different stirring times and speeds (rapid for mixing coagulant and slow for coagulation) to be preset. 800 mL of the test solution described above was transferred to a 1-L beaker. Under rapid stirring conditions, 0.40 ml of the stock kaolin suspension was added by using a micro-pipette, giving a clay concentration of 50 mg/L. 5 ml of the stock HA (commercial products from Tianjin, China) solution was added to give a HA concentration of 2 mg/L. The coagulation experiments were conducted at room temperature (23–26 °C). Prior to the addition of coagulants, the target pH was adjusted by adding a predetermined amount of NaOH or HCl into the kaolin suspension, with rapid stirring. The coagulant was added using a micropipette. After dosing, one minute rapid mixing at 250 rpm was applied, followed by 15 min slow stirring at 40 rpm. The flocs were allowed to settle for 10 min and the residual turbidity (RT) was measured using a Hach Ratio/XR turbidimeter. Another quantity of samples were taken and pre-filtered using 0.45 μm membrane to measure absorbance at 254 nm using a TM8500 UV-Vis spectrophotometer. The pH of the supernatant was also measured. A small sample was taken immediately after the 1-minute rapid mix period for determination of electrophoretic mobility.

Results and discussion

Characterization of Al_{13} nano-floccculant

The results of ferron assay for the Al_{13} solutions prepared are listed in Table 2.

Al_t means total Al(III) concentration, Al_a means the fraction reacted suddenly within 1 min, Al_b as the fraction reacted quickly between 1 min and 2 h, and Al_c the last unreacted fraction.

It can be seen that the samples prepared at concentrations of 0.01–2.0 mol Al/L contain mainly Al_b species, i.e. more than 97%. No Al_c fraction exists significantly as the ferron method has the analytical error around 1%. It seems also that the Al_a fraction could be contributed from surface Al of Al_{13}, i.e. as the results of the rapid dissolution/dissociation of surface Al by ferron. It should be noted that the speciation characterization by ferron method is operationally defined, i.e., Al_a is the fraction reacted suddenly in 1 min. Some researchers define the Al_a fraction reacted in 30 s. Therefore, the Al_a calculated here is significantly higher. The samples obtained contain therefore mainly Al_{13} species. It indicates that the Al_{13} samples prepared can be diluted into various concentrations. High concentration Al_{13} solutions are relatively stable and therefore become the valid proof for a commercial preparation.

Figure 1 is the results of Al_{13} characterization by using ^{27}Al-NMR. It is obvious that the ^{27}Al-NMR figures exhibit only a sharp single response at 63.0 ppm. No peak of Al_m (monomer) at 0 ppm or other species can be observed for all the samples. And the peak area at 63.0 ppm increases rapidly with the increase of concentration. A very good linear

Table 2 The speciation distribution of purified Al_{13} solutions by ferron assay

Al_t (molAl/l)	Al_a%	Al_b%	Al_c%
0.01	2.35	97.44	0.20
0.055	2.20	97.77	0.03
0.11	2.31	97.33	0.36
0.42	2.06	97.38	0.56
1.06	2.02	96.80	1.18
2.11	1.91	96.59	1.60

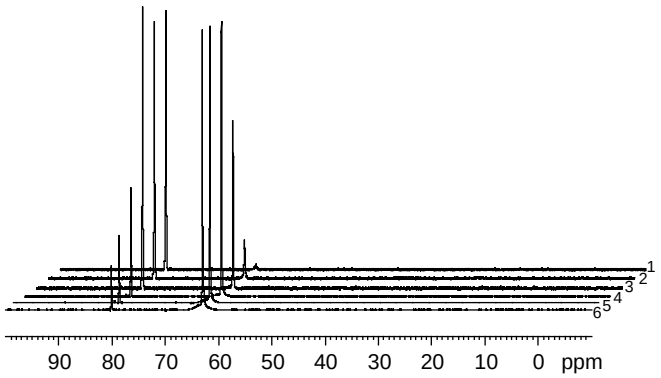

Figure 1 Characterization of the pure Al_{13} by ^{27}Al-NMR (the Al_t for the 1, 2, 3, 4, 5, and 6 samples is 0.01, 0.055, 0.11, 0.42, 1.06, and 2.11 molAl/l respectively)

equation with R^2 of 0.9996 can be yielded, i.e., $y = 4.085x + 0.0231$, where y is the peak area, and x is the concentration. It indicates that the only species observed in the above samples are Al_{13}. The results show that the Al_{13} detected by ^{27}Al-NMR has a good relation with Al_b under these conditions. The Al_{13} solution was further characterized by using AFM. It provides the direct morphology observation for purified Al_{13}.

The sample of 0.1 mol/L is shown in Figure 2. It seems that the purified Al_{13} is quite stable and as the basic structure unit to form fractal aggregates. The fractal aggregation feature has also been observed by Bottero *et al.* with SAXS. Further comparison of Al_{13} with PACl samples has been addressed elsewhere. The solid powder of purified Al_{13} sample and sulfate salts have been analysed by IR. The IR spectrum is shown in Figure 3. It can be seen that the frequency between 3,500–3,400 cm^{-1} is the vibration of –OH group reflecting typically the complexation of OH-Al. And the frequency at 2,400 cm^{-1} or so is the vibration of Al-O, and 1,640 cm^{-1} shown as the structure combined water. The frequencies between 1,000–400 cm^{-1} are the vibration of surface –OH group. The figures exhibit largely similar features for the Al_{13} powder and its sulfate salts except that the latter shows a typical S-O vibration at 1,117 cm^{-1}.

Effect of dose and pH on coagulation of HA

The effects of dose and pH on coagulation of HA with various coagulants were investigated and the results under dose of 2×10^{-5} and 1×10^{-4} mol/L are shown in

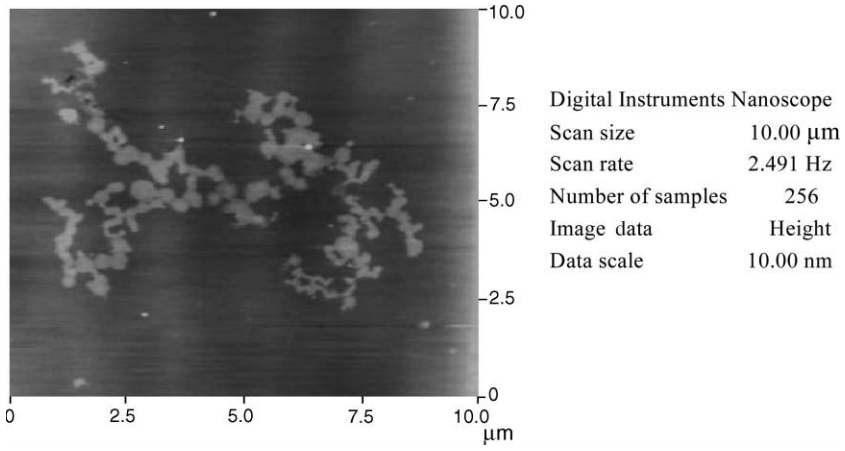

Figure 2 The AFM observation of Al_{13} sample

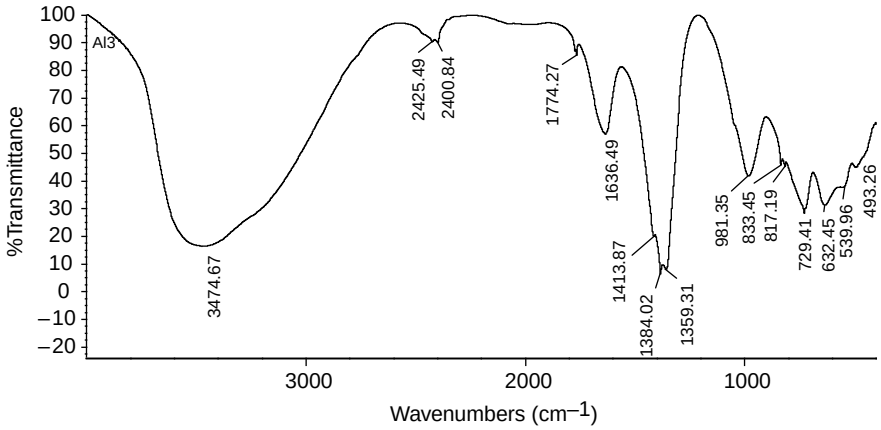

Figure 3 The IR spectrum of solid Al_{13} sample

Figures 4 and 5 respectively. The changes of the zeta potential, RT and UV_{254} with pH are shown in Figures 4a–c. Under the dosage of 2×10^{-5} mol/L, the first zero charge point of pH (pH_{zcp}) for $PACl_0$ appears at 4.10. And the zeta potential becomes the largest at 5.19. Sequentially the pH_{zcp} appears for the $PACl_0$, $PACl_{ind}$, $PACl_{25}$, Al_{13} at 6.81, 7.00, 7.06 and 7.52 respectively. Increase pH to 8.44, the difference among the various coagulants disappears gradually and finally reaches a platform of -49 mV.

From Figure 4b, it can be seen that the change of RT corresponds well with the change of zeta potential. The bulk system becomes destabilized when reaching pH_{zcp}. Only $PACl_0$ exhibits two zones for coagulation with two pH_{zcp}. The system becomes restabilized at acidic or high pH region for the other PACl coagulants. The removal of HA as shown from the change of UV_{254} (Figure 4c) exhibits slight difference with the change of zeta potential and RT. It is better removed at low pH area and becomes deteriorated at pH higher than 7.20. It is indicative that flocs formed at different particle size at acidic region but are removed well after membrane filtration during the UV_{254}

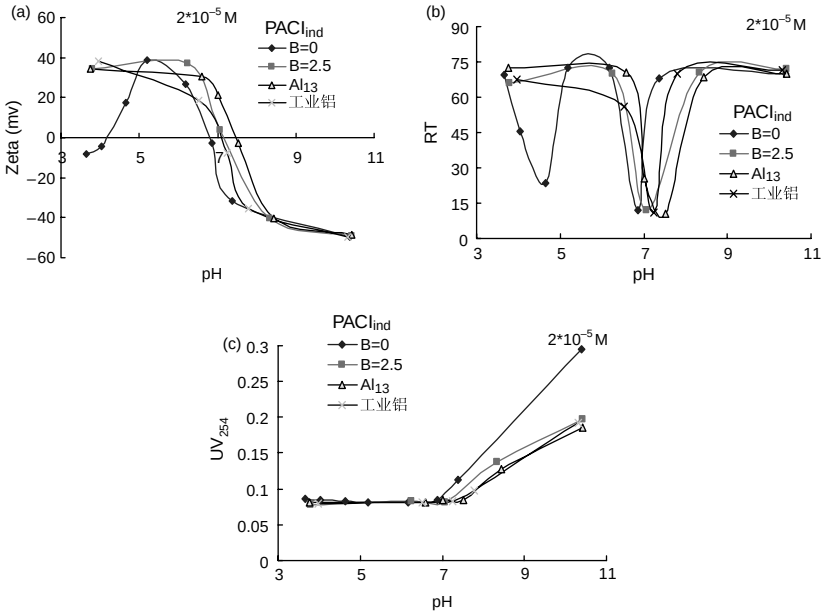

Figure 4 The change of zeta, RT and UV with pH (2×10^{-5} mol/L)

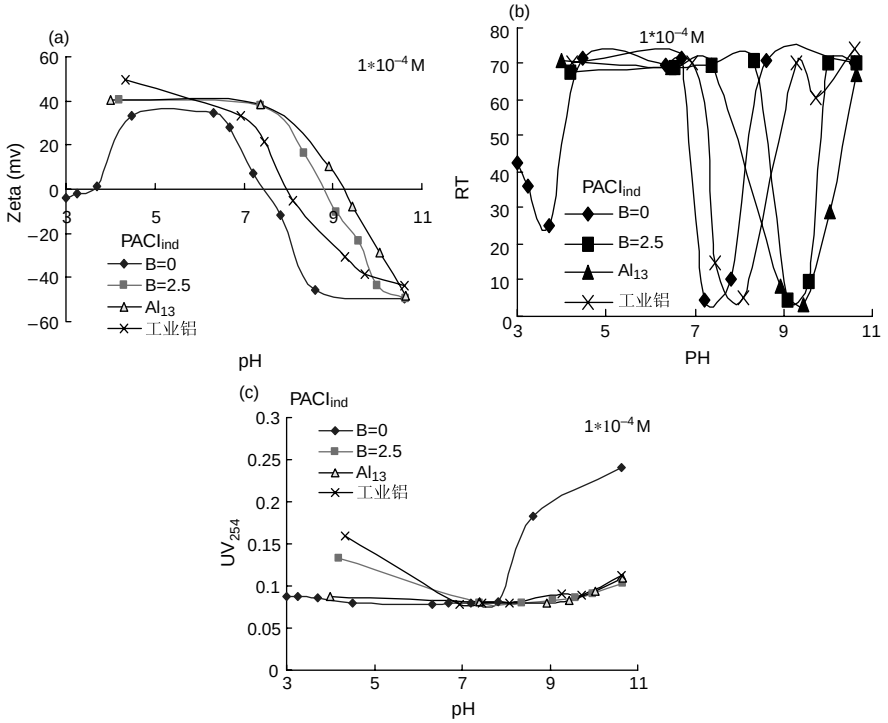

Figure 5 The change of zeta, RT and UV with pH (1×10^{-4} mol/L)

measuring. In the high pH region, it can be observed that the different coagulants exhibit quite different behavior. The Al_{13} exhibits the best HA removal, with the second of $PACl_{25}$, and then the $PACl_{ind}$ and $PACl_0$ subsequently. Increase the dose of coagulants to 5×10^{-5} mol/L (data not shown), the phenomenon appears almost the same.

Further increase the dose to 1×10^{-4} mol/L and the results are shown in Figure 5. It is observed the first zero charge point of pH (pH_{zcp}) for $PACl_0$ moves to the acid side and appears at 3.70. And the zeta potential becomes the largest between 4.5 and 6.5 for $PACl_0$. While for $PACl_{ind}$, $PACl_{25}$ and Al_{13}, it remains at 7.0, 7.2 and 7.2 respectively. Sequentially the pH_{zcp} appears again for the $PACl_0$, and $PACl_{ind}$, $PACl_{25}$, Al_{13} at 7.50, 8.00, 8.80 and 9.20 respectively. Different from the low dosage, the variation in zeta potential among the coagulants disappears and reaches a platform only when the pH increases to 10.50. From Figure 5b, it can also be seen that the change of RT corresponds well with the change of zeta potential. Compared with the system at lower dosage, the destabilization and restabilization zones become wider, i.e., extending to much lower acidic and higher basic region. It becomes more evidently from the removal of HA as shown from the change of UV_{254} (Figure 5c). In the high pH region, it can be observed that the difference among coagulants disappears except for $PACl_0$. It indicates that the PACl being preformed exhibits efficient reaction with HA and the effect of pH becomes less.

Discussion: role of Al_{13} on coagulation

The above results show that the effect of the dose in this case exhibits mainly in the wider coagulation zone and extends to the higher pH region. However, the speciation of coagulants has a significant role.

For the aluminium salt, the efficiency of coagulation depends largely on the pH. The hydrolysis products formed after dosing and their charge feature varies markedly with the

solution pH. With the increase of pH, the hydrolysis of Al(III) undergoes multiple reactions along with hydrolysis-polymerization-precipitation and dissolving as well. And the multi-reaction paths such as co-precipitation, surface hydrolysis/polymerization and precipitation will occur under the typical conditions. Under pH of 4.0, the main species are monomers which exhibit low charge-neutralization ability. While for PACl, the preformed polymer has high charge neutralization ability. The suspension remains stabilized.

Within $4.00 < pH < 7.00$, the hydrolysis products of Al(III) are weakly charged amorphous $Al(OH)_3$ and some polymer species might also be formed (Tang, 1998). The system becomes restabilized with large amounts of low particle size floc formed. The aggregates formed differ little with the various coagulants. However, the more Al_{13} is preformed, the easier and higher-charged are flocs formed. This becomes more evident with the increase of pH to the higher basic region. The pH_{zcp} for the reaction products, i.e., floc aggregates, reaches subsequently for $PACl_0$, $PACl_{ind}$, $PACl_{25}$ and Al_{13} in accordance with the amount of Al_b/Al_{13} as shown in Table 1.

From the total coagulation and restabilization phenomenon of the system, it can be seen that the Al_{13} species exhibit highly efficient charge-neutralization ability. Being preformed, the Al_{13} are quite stable. The high charge loading feature accompanies the speciation stability well (Tang, 1998). It can be directly absorbed into the particle surface and form bridge among particles as well. With the increase of solution pH, the Al_{13} can aggregate into large fractal aggregates and act continuously as the bridge-sweep function. The hydrolysis of Al(III) depends largely on the solution conditions. In the basic region the aluminium salt becomes dissolved into the $Al(OH)_4^-$ species and exhibits no coagulation effect any more. The $PACl_{25}$ cannot evaluate its coagulation efficiency with simply the content of Al_{13}, a 'patch coagulation effect' might be involved as indicated with the fractal aggregates of Al_{13} (Pinnavia, 1983).

Conclusions

The results obtained show that the Al_{13} has efficient speciation stability. The nano-Al_{13} flocculant can be tailor-made in various concentrations up to 2.0 mol/L as examined. Under the suspension system containing HA, the change of pH has only a slight effect on the coagulation behavior of Al_{13} compared with the Al(III) salt. The Al_{13} exerts a significant charge-neutralization effect immediately after dosing. At higher pH, fractal aggregates of Al_{13} can be formed keeping the acid-base feature of Al_{13} and efficient coagulation.

Acknowledgements

This work is supported by the national 863 program under 2002AA001290, the 'Preparation of Al_{13} Nano-flocculant', and also the NSF of China under 20477054.

References

Bertsch, P.M. (1996). *The Environmental Chemistry of Aluminum*, Chapter 4, CRC Press, Boca Raton, FL, USA.

Furrer, G. (1993). New aspects on the chemistry of aluminum in soils. *Aquat. Sci.*, **55**, 281.

Gray, K.A., Yao, C.H. and O'Melia, C.R. (1995). *J. Am. Water Wks Assn.*, **87**(4), 136.

Matsui, Y., Yuasa, A., Furuya, Y. and Kamei, T. (1996). *J. Am. Water Wks Assn.*, **88**(10), 96–106.

Parker, D.R. and Bertsch, P.M. (1992). Identification and quantification of the "Al_{13}" tridecameric polycation using ferron. *Environ. Sci. Technol.*, **26**, 908.

Parthasarathy, N. and Buffle, J. (1985). Study of polymeric aluminum(III) hydroxide solutions for application in waste water treatment. Properties of the polymer and optimal conditions for preparation. *Wat. Res.*, **19**, 25.

Pinnavia, T.J. (1983). Intercalated clay catalysts. *Science*, **220**, 365.
Tang, H.X. (1998). The flocculation morphology of hydroxyl polyaluminum chloride. *Acta Circum. Sinica*, **18**(1), 1–10 (in Chinese).
Tang, H.X. and Luan, Z.K. (1996). The different behavior and mechanism between inorganic polymer flocculant and traditional coagulants. Hahn, H.H. *et al*. (eds), *Chemical Water and Wastewater Treatment (IV)*, Springer-Verlag, pp. 83–93.
Teagarden, D.L., Kozlowski, J.F., White, J.L. and Hem, S.L. (1981). Aluminum chlorohydrate I. Structure studies. *J. Pharm. Sci.*, **70**, 758.
Wang, D.S., Tang, H.X. and Gregory, J. (2002). Relative importance of charge-neutralization and precipitation during coagulation with IPF-PACl: Effect of sulfate. *ES&T*, **36**(8), 3866.
Wang, D., Sun, W., Xu, Y., Tang, H. and Gregory, J. (2004). Speciation stability of inorganic polymer flocculant-PACl. *Colloid Surf.*, **243**, 1–10.
Van Benschoten, J. and Edzwald, J.K. (1990). Chemical aspects of coagulation using aluminum salts I. Hydrolytic reactions of aluminum and polyaluminum chloride. *Wat. Res.*, **24**(12), 1519.
Xu, Y., Dongsheng, W., Hong, L. and Hongxiao, T. (2003). Optimization on the separation and purification of Al_{13}. *Colloid Surf.*, **231**, 1–9.